Astronomy & Astrophysics

Constraints on the near-Earth asteroid obliquity distribution from the Yarkovsky effect

C. Tardioli[1], D. Farnocchia[2], B. Rozitis[3], D. Cotto-Figueroa[4], S. R. Chesley[2], T. S. Statler[5,6], and M. Vasile[1]

[1] Department of Mechanical & Aerospace Engineering, University of Strathclyde, Glasgow, G1 1XJ, UK
    e-mail: Chiara.Tardioli@strath.ac.uk
[2] Jet Propulsion Laboratory, California Institute of Technology, Pasadena, CA 91109, USA
[3] School of Physical Sciences, The Open University, Milton Keynes, MK7 6AA, UK
[4] Department of Physics and Electronics, University of Puerto Rico at Humacao, 00792 Humacao, Puerto Rico
[5] Department of Astronomy, University of Maryland, College Park, MD 20742, USA
[6] Planetary Science Division, Science Mission Directorate, NASA Headquarters, Washington, DC 20546, USA

ABSTRACT

Aims. From light curve and radar data we know the spin axis of only 43 near-Earth asteroids. In this paper we attempt to constrain the spin axis obliquity distribution of near-Earth asteroids by leveraging the Yarkovsky effect and its dependence on an asteroid's obliquity.
Methods. By modeling the physical parameters driving the Yarkovsky effect, we solve an inverse problem where we test different simple parametric obliquity distributions. Each distribution results in a predicted Yarkovsky effect distribution that we compare with a χ^2 test to a dataset of 125 Yarkovsky estimates.
Results. We find different obliquity distributions that are statistically satisfactory. In particular, among the considered models, the best-fit solution is a quadratic function, which only depends on two parameters, favors extreme obliquities consistent with the expected outcomes from the YORP effect, has a 2:1 ratio between retrograde and direct rotators, which is in agreement with theoretical predictions, and is statistically consistent with the distribution of known spin axes of near-Earth asteroids.

Key words. methods: statistical – celestial mechanics – minor planets, asteroids: general

1. Introduction

The complex motion of near-Earth asteroids (NEAs) is dominated by the gravitational perturbations of the Sun and planets. However, the gravitational interaction with other small bodies and non-gravitational perturbations can affect their behavior and become relevant for the prediction of their future positions (Farnocchia et al. 2015).

In particular, the Yarkovsky effect is a subtle non-gravitational acceleration due to the anisotropic emission of thermal radiation of Solar System objects that causes a secular drift in the semi-major axis (Bottke et al. 2006). This perturbation is important to understand the long-term dynamics of the asteroid population since it is a driving factor for feeding resonances in the main belt and transporting asteroids to the inner Solar System (Farinella et al. 1998; Morbidelli & Vokrouhlický 2003; Bottke et al. 2002b). The Yarkovsky effect is also relevant for impact hazard predictions where high-precision ephemeris predictions are required (Giorgini et al. 2002, 2008; Chesley 2006; Farnocchia et al. 2013b; Farnocchia & Chesley 2014; Chesley et al. 2014; Spoto et al. 2014; Vokrouhlický et al. 2015b).

The diurnal component of the Yarkovsky effect, which is usually the dominant one, is proportional to the cosine of the obliquity of the spin axis (Bottke et al. 2006). Therefore, the spin orientation determines whether an asteroid's semi-major axis drifts inwards or outwards. More than ten years ago, La Spina et al. (2004) analyzed the distribution of known NEA

spin axes, about 21 at the time, and found a $2^{+1}_{-0.7}$ ratio of retrograde to direct rotators. The observed ratio was an excellent match to the one expected from the Bottke et al. (2002a) NEA population model and the injection mechanism of asteroids to the inner Solar System through orbital resonances, that is, 2 ± 0.2.

A derivation of the Yarkovsky accelerations from thermophysical modeling is generally impractical as they depend on physical properties such as size, mass, shape, obliquity, and thermal properties (Bottke et al. 2006) and even the surface roughness (Rozitis & Green 2012), which are generally unknown. However, for asteroids with a well-observed astrometric arc, it is possible to directly estimate the Yarkovsky effect by measuring deviations from a gravity-only trajectory (Chesley et al. 2003, 2016; Vokrouhlický et al. 2008, 2015a; Nugent et al. 2012; Farnocchia et al. 2013a, 2014).

We currently have a limited dataset of known NEA spin axes; the EARN[1] and the DAMIT[2] databases combined list 43 as of Mar 9, 2017. Thus, it is difficult to derive a statistically reliable obliquity distribution. In general, one needs specific observations at multiple observing geometries to constrain the spin axis of an asteroid, for example, light curves (Ďurech et al. 2009, 2011) or radar observations (Benner et al. 2015). Even so, in many cases there are two distinct solutions and it is not always possible to identify the correct one. An interesting example

---

[1] http://earn.dlr.de/nea/
[2] http://astro.troja.mff.cuni.cz/projects/asteroids3D/web.php

is (29075) 1950 DA, which had two possible pole solutions from radar observations (Busch et al. 2007). The estimate of the Yarkovsky effect on this object (Farnocchia & Chesley 2014) resolves the ambiguity between the two in favor of the retrograde solution.

Along the same lines, in this paper we use a current dataset of Yarkovsky estimates to put constraints on the NEA obliquity distribution. In particular, by using the properties of the NEA population we can derive distributions from most of the parameters on which the Yarkovsky effect depends. By making numerous assumptions, for example, neglecting the dependence of the Yarkovsky effect on bulk density and thermal properties, Farnocchia et al. (2013a) made a previous attempt to infer a four-bin NEA obliquity distribution from a set of 136 Yarkovsky detections. In this paper we use a more sophisticated technique by solving an inverse problem where different obliquity distributions are tested to provide the best match to the Yarkovsky estimate dataset. This technique was introduced, with a preliminary application to a similar dataset, in Cotto-Figueroa (2013).

2. Yarkovsky modeling

The Yarkovsky perturbation can be modeled as a transverse acceleration A_2/r^2 (Farnocchia et al. 2013a), where r is the distance from the Sun in au and A_2 is the sum of two terms, one corresponding to the diurnal effect due to the asteroid's rotation and one corresponding to the seasonal effect due to the asteroid's orbital motion:

$$A_2 = \frac{4(1-A)}{9} \Phi(1 \text{ au}) \left[\alpha f(\theta_{\text{rot}}) \cos \gamma - \frac{1}{2} f(\theta_{\text{rev}}) \sin^2 \gamma \right], \quad (1)$$

where A is the Bond albedo, $\Phi(1\text{au}) = 3G_S/(2D\rho c)$ is the standard radiation force factor at 1 au, $G_S = 1361$ W/m^2 is the solar constant, D is the asteroid's diameter, ρ is the bulk density, and γ is the spin obliquity. The thermal parameters θ_{rot} and θ_{rev} depend on the rotation and revolution periods, respectively, and also on spin rate, thermal inertia, thermal emissivity, geometric albedo p_{v}, and r. The function f describes the spin-rate and thermal-inertia dependence of the Yarkovsky acceleration for a Lambertian sphere, it is non-monotonic and $f(0) = f(\infty) = 0$ (Bottke et al. 2006). Finally, α is an enhancement factor that is intended to describe the effect of surface roughness alone, but that effect is itself dependent on thermal inertia and spin rate (Rozitis & Green 2012).

By separating the obliquity γ from all of the other parameters we have

$$A_2 = F_1(D, A, \rho, \Gamma, \bar{r}, P_{\text{rot}}, \alpha) \cos \gamma + F_2(D, A, \rho, \Gamma, \bar{r}, P_{\text{rev}}) \sin^2 \gamma, \quad (2)$$

where F_1, F_2 are positive functions that do not depend on the obliquity. To simplify we replace the instantaneous heliocentric distance with the solar flux-weighted mean heliocentric distance $\bar{r} = a\sqrt{1 - e^2}$, where a and e are orbital semi-major axis and eccentricity, respectively. Equation (2) represents the starting point of our inverse process to derive possible obliquity distributions starting from probability distributions for A_2, D, A, ρ, Γ, $\bar{r}$, P_{rot}, P_{rev}, and α.

3. Dataset of Yarkovsky estimates

To obtain a distribution of A_2 on the left-hand side of Eq. (2) we used the Chesley et al. (2016) list of Yarkovsky estimates. This
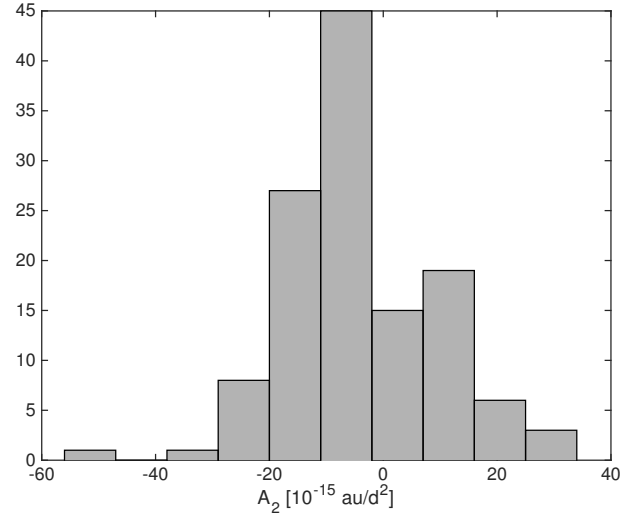
Fig. 1. Histogram of Yarkovsky estimates normalized by an absolute magnitude scale factor of 1329 km $10^{-H/5}/\sqrt{0.154}$. The average 1σ uncertainty in normalized A_2 is 5×10^{-15} au/d^2.

list contains 42 Yarkovsky detections considered "valid", which means that the signal-to-noise ratio (SNR) of the detection is greater than 3 and its value is compatible with the Yarkovsky mechanism.

Moreover, Chesley et al. (2016) have a second category referred to as "weak" detections where the Yarkovsky estimate uncertainty is small enough that it would permit a clear detection if the Yarkovsky A_2 parameters were scaled from that of Bennu using its $1/D$ dependence. However, the astrometric observations are incompatible with such accelerations thus suggesting a lower magnitude of the Yarkovsky effect. Some of Bennu's physical properties tend to increase the Yarkovsky effect, for example, the extreme obliquity of 178° and the low bulk density of 1.3 g/cm^3 (Chesley et al. 2014), thus the category of "weak" detections is likely to include objects that have physical properties (e.g., obliquity, bulk density) that lower the magnitude of the Yarkovsky effect. We included these "weak" detections in our dataset to avoid biasing the sample against non-extreme obliquities.

We updated the Chesley et al. (2016) list by including all of the available optical and radar astrometry as of September 2016, for a final dataset of 125 Yarkovsky estimates (see Table A.1). To limit the spread in A_2 caused by the diverse sizes (from a few meters to a kilometer in diameter) of the objects for which we have a Yarkovsky estimate, we normalized the A_2 values by an absolute magnitude scale factor 1329 km $10^{-H/5}/\sqrt{p_{\text{v}}}$ with a constant albedo $p_{\text{v}} = 0.154$. The resulting A_2 distribution is shown in Fig. 1.

4. Probability distribution of physical parameters

To invert Eq. (2) and solve for an obliquity distribution, we need to model the intrinsic distributions of the other parameters needed to compute the Yarkovsky effect, that is, D, A, ρ, Γ, $\bar{r}$, P_{rot}, P_{rev}, and α. The adopted distributions are based on what is known of the NEA population as well as the specific properties of the Yarkovsky estimate dataset.

Diameter. To derive the diameter we use the standard conversion formula from absolute magnitude H and geometric albedo p_{v} (Pravec & Harris 2007):

$$D = 1329 \frac{10^{-H/5}}{\sqrt{p_{\text{v}}}}. \quad (3)$$
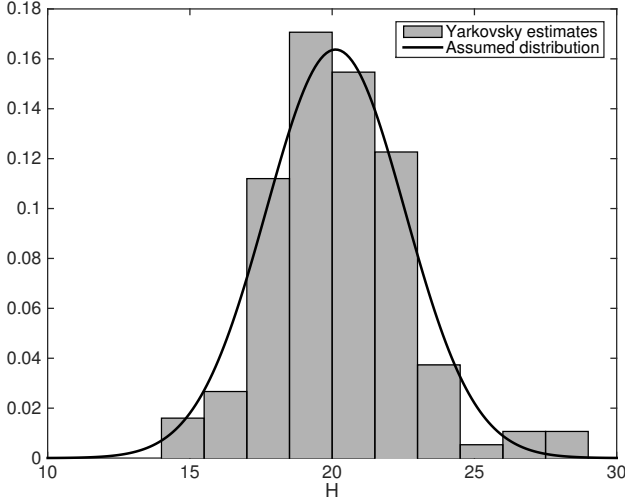
Fig. 2. Probability distribution of the absolute magnitude for the objects in Table A.1.

**Table 1.** Geometric albedo, bulk density and frequency for different taxonomic classes in an H-limited sample.

Class	p_v	ρ (g/cm^3)	Frequency
C	0.06 ± 0.05	1.5 ± 0.5	16%
S	0.18 ± 0.05	2.5 ± 0.5	62%
X	0.30 ± 0.10	2.8 ± 0.7	22%

Notes. The table reported the median m and standard deviation s of lognormal distributions. The mean and standard deviation of the associated normal distribution are calculated as $\mu = \ln(m)$ and σ such that $(e^{\sigma^2} - 1)e^{2\mu+\sigma^2} = s^2$.

While the absolute magnitude distribution of NEOs follows a power law (Bottke et al. 2002a), the one of the objects in our dataset of Yarkovsky estimates resembles a normal distribution; see Fig. 2. The shape of the distribution can be explained by the contribution of two factors: on one side there are fewer bigger objects in the population, and on the other side there are smaller objects, which are faint and so are harder to observe or even discover. Therefore, small objects are less likely to have long observation arcs, which reduces the chances of obtaining constraints on the Yarkovsky effect. The result is that objects with a magnitude around $H = 20$ are currently the ones more likely to have a Yarkovsky estimate. To sample H we selected a normal distribution with a mean of 20.12 and standard deviation of 2.44.

Geometric albedo. For the geometric albedo we consider three major taxonomic classes: C, S, and X. The split and frequencies are from Chesley et al. (2002) with the difference that we combine the M-class and the E-class into X. For each of the classes, we use lognormal distributions with median and standard deviation shown in Table 1, which are informed by the statical analysis presented in Thomas et al. (2011). The usage of lognormal distributions prevents the occurrence of nonphysical negative values of p_v. From the drawn values of H and p_v we sample the diameter using Eq. (3).

Among the objects of Table 1, only 39 objects have known taxonomy in the C, S, and X classes. The split is consistent with that of Table 1, in fact $(7.7 \pm 4.1)\%$ are of type C, $(74 \pm 7.0)\%$ are of type S, and $(17.7 \pm 6.2)\%$ are of type X.
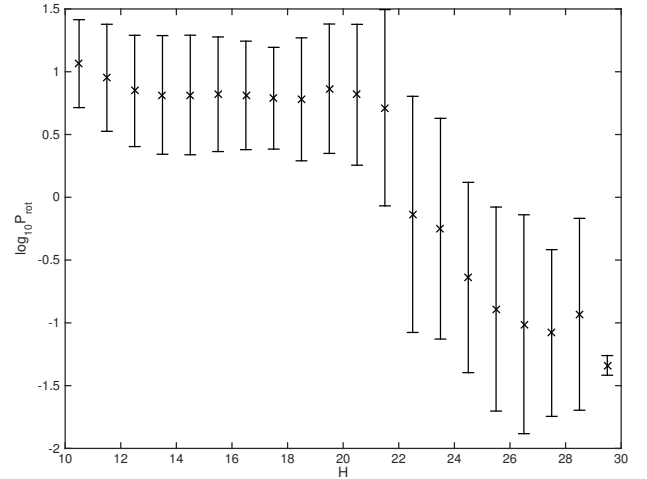
Fig. 3. Median (crosses) and 1σ standard deviation of the rotation periods from the JPL Small-Body Database for bins of 1 mag from $H = 10$ to $H = 30$.

Bond albedo. The Bond albedo A is a function of the geometric albedo p_v and the slope parameter G: $A = (0.29 + 0.684G)p_v$ (Bowell et al. 1989). We already described the distribution for p_v. Following Mommert et al. (2014a) and Mommert et al. (2014b), we analyzed the current statistics from the JPL Small-Body Database[3] and obtained normal distribution for G with a mean 0.18 and a standard deviation 0.13. The geometric albedo was derived from the distributions described earlier.

Bulk density. Similar to what was done for the geometric albedo, for the bulk density ρ we considered lognormal distributions depending on the taxonomic class; see Table 1. The distribution parameters are based on the census of asteroid densities performed by Carry (2012). We note that, once the taxonomic class is drawn, the distributions of both p_v and ρ are chosen consistently with that taxonomic class, thus accounting for the fact that p_v and ρ are not independent.

Thermal inertia. To account for thermal inertia, we computed the thermal parameter for each NEA with a measured thermal inertia value from Table 2 of Delbò et al. (2015). We excluded (54509) YORP from this list because of the very large uncertainty on its derived thermal inertia value. A lognormal distribution was then fit to the 13 measured thermal parameter values to give the mean NEA thermal parameter as $\theta_{rot} = 10^{0.6\pm0.3}$. For our synthetic population, thermal parameters were then randomly drawn from this log-normal distribution.

Rotation period. The rotation period P_{rot} is size dependent. In particular, there is the so-called spin barrier of 2.2 h (Warner et al. 2009): few objects with $H < 20$ spin faster than this limit. Therefore, we divide the absolute magnitude in bins of 1 mag and for each bin we sample the rotation period according to the mean and standard deviation of the rotation periods available from the JPL Small-Body Database (most of which are from the Warner et al. 2009, asteroid light curve database) in that bin (see Fig. 3). To avoid nonphysical values of the rotation period, we removed samples with a period greater than 1000 h. Moreover, we removed the samples with a rotation period smaller than 2 h for $H \leq 20$, or smaller than 0.01 h for $H > 20$.

Orbital period and solar-flux-weighted heliocentric distance. Some orbital configurations favor a Yarkovsky estimate, for example, potentially hazardous asteroids (PHAs) are more likely to come close to Earth and so are easier to observe,

---

[3] http://ssd.jpl.nasa.gov/sbdb_query.cgi
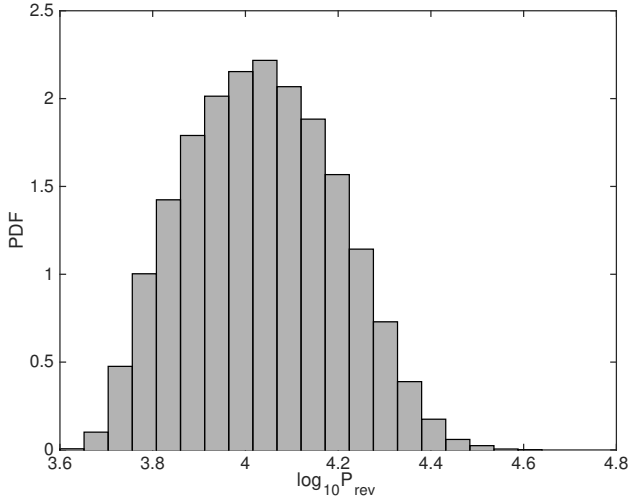
Fig. 4. Orbital period distribution as derived from the objects in Table A.1.

especially using radar. In particular, none of the objects in the dataset has a perihelion $q > 1.15$ au or an aphelion $Q < 1$ au. Since the orbital geometry can introduce a selection effect, we took the distribution in semi-major axis a and e corresponding to our set of Yarkovsky detections: the semi-major axis distribution is approximated with a lognormal distribution whose associated normal distribution has mean 0.13 au and standard deviation 0.33 au, while the eccentricity distribution is approximated with a normal distribution with mean 0.4 and standard deviation 0.2 truncated at 0 and 1. Finally, we filtered out the objects with $q > 1.15$ au and $Q < 1$ au, and converted the semi-major axis to the orbital period P_{rev} (see Fig. 4).

The distribution in solar-flux-weighted heliocentric distance $\bar{r}$ is derived from the a and e distributions described above.

Enhancement factor. Small-scale surface roughness enhances the diurnal component of the Yarkovsky effect through thermal-infrared beaming, that is, re-radiation of absorbed sunlight back towards the Sun (Rozitis & Green 2012). The degree of enhancement is a non-linear function of the asteroid thermal parameter, albedo, and heliocentric distance. In particular, it has been previously shown that the enhancement factor increases for decreasing thermal parameter and decreasing heliocentric distance, and it also increases for increasing albedo. The enhancement factor for a set of properties can be calculated for a spherically shaped asteroid covered with hemispherical craters (i.e., the craters represent the surface roughness) using the thermophysical model described in Rozitis & Green (2012).

Using this model, we generated a lookup table to obtain the enhancement factor as a function of A, θ_{rot}, and $\bar{r}$. The top panel of Fig. 5 shows the enhancement factor corresponding to a 100% roughness as a function of θ_{rot}. Finally, we obtain α by scaling by the asteroid's surface roughness, which is uniformly drawn between 0% and 100%. On average we obtain a 15% enhancement of the diurnal component of the Yarkovsky effect. The bottom panel of Fig. 5 shows the resulting distribution of α, obtained from the drawn A, θ_{rot}, and $\bar{r}$ and interpolating the lookup table.

5. Models for the obliquity distribution

We considered three different parametric models for the distribution of the cosine of the obliquity. These parametric formulations enable us to generate synthetic A_2 distributions to be compared to the Yarkovsky dataset of Sect. 3 and in turn find the ones
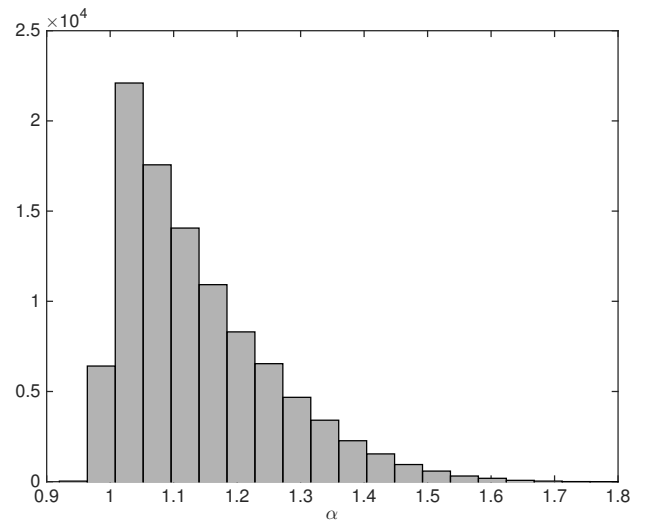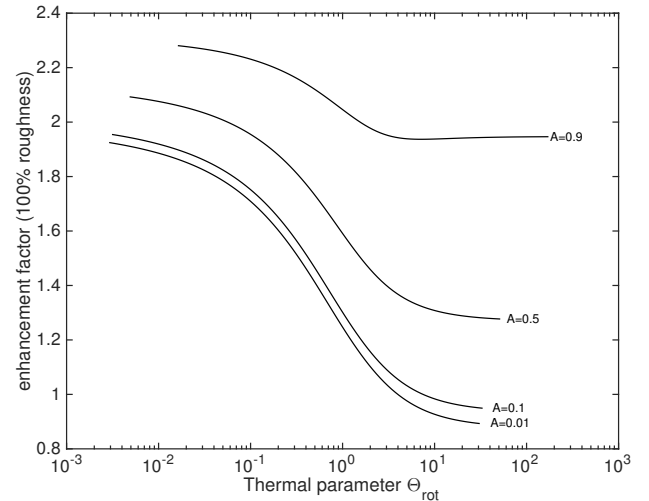
Fig. 5. *Above*: enhancement factor α corresponding to 100% roughness as a function of the thermal parameter. The level curves correspond to a distance of 1 au. *Below*: histogram of the enhancement factor α.
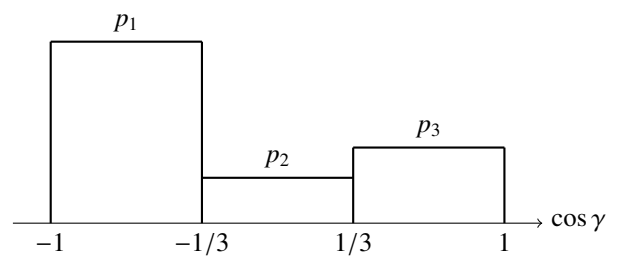
Fig. 6. Example of a three-bin distribution.

providing the best match. Because of the YORP effect, we expect local maxima of the distribution for extreme obliquities (0° and 180°) and a minimum close to $\gamma = 90°$ (Čapek & Vokrouhlický 2004).

Bin model. The simplest model considers a number of bins N and tests different frequencies p_i, $i = 1, N$ for each bin. Each p_i has to be positive and their sum has to be 1. The number of degrees of freedom is $N - 1$. Figure 6 shows an example with $N = 3$.

Piecewise linear model. The second model we considered is that of a continuous piecewise linear (PL) function, as shown in Fig. 7. The three parameters defining this distribution are the
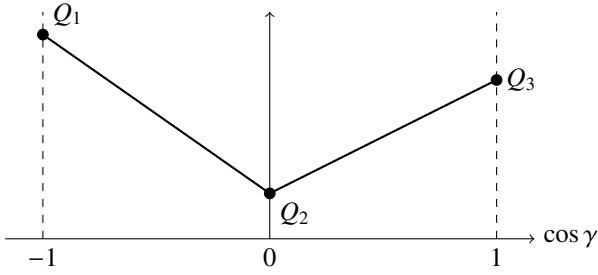
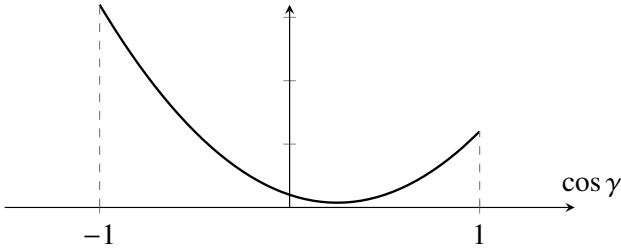**Fig. 7.** Example of a piecewise linear distribution.

Fig. 8. Example of a quadratic distribution.

ordinates Q_1, Q_2, and Q_3 in -1, 0, and 1, respectively. Since the integral has to be one, that is, $Q_1 + 2Q_2 + Q_3 = 2$, the number of independent parameters is 2. This model can be generalized by having a variable abscissa x_2 for the middle point, thus leading to three independent parameters. We refer to this generalization as PLMP.

Quadratic model. The final model we consider is that of a quadratic function $f(\gamma) = a\cos^2\gamma + b\cos\gamma + c$ (see Fig. 8). We allow only concave-up parabolas, that is, $a > 0$, as we know that the YORP effect favors extreme obliquities (Čapek & Vokrouhlický 2004). The parabola's minimum must be positive and its abscissa between -1 and 1, and the integral has to be 1. Therefore, the number of independent parameters is 2.

6. Solution of the inverse problem

Starting from the distributions described in Sect. 4 and a given parametric distribution in the obliquity, we can draw samples and use Eq. (2) to obtain samples in A_2 (see Fig. 1). Therefore, for each parametric obliquity distribution we obtain a predicted distribution in A_2 to be compared with that coming from the set of Yarkovsky estimates. As already described in Sect. 3, the A_2 values are normalized by absolute magnitude to reduce the spread caused by the range of different sizes considered.

To measure how well the predicted distribution matches the one from the Yarkovsky estimates we perform a χ^2 test. The range of normalized A_2 values is divided in m bins so that each bin contains the same probability mass from the predicted distribution, that is, the integral of the predicted distribution over each bin is $1/m$. Then, from the list of Yarkovsky estimates we compute the probability $p_i, i = 1, m$ of falling within each bin. Finally, χ^2 is computed as:

$$\chi^2 = \sum_{i=1}^{m} \frac{(p_i - 1/m)^2}{1/m}. \tag{4}$$

We look for the obliquity distributions providing a lower χ^2, which from standard χ^2 statistics should be close to $m - 1 - n_p$,
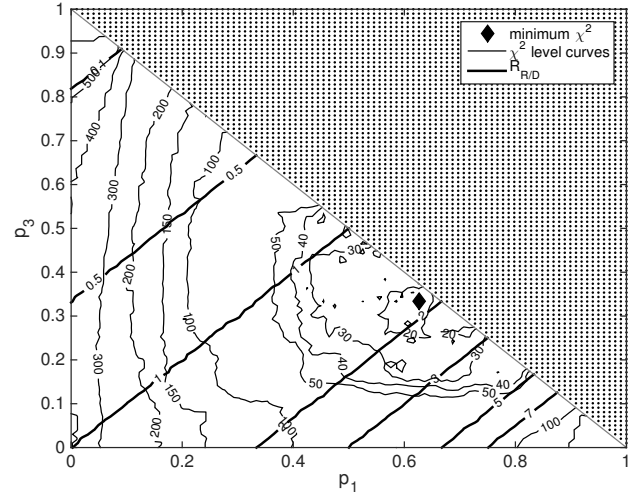

Fig. 9. Discrete three-bin distribution. Thin lines indicate level curves of χ^2 in the two-dimensional (2D) search space. The minimum χ^2 is marked with a diamond. Thick lines mark loci of constant retrograde to direct rotator ratios. The dotted area corresponds to inadmissible values of the parameters.
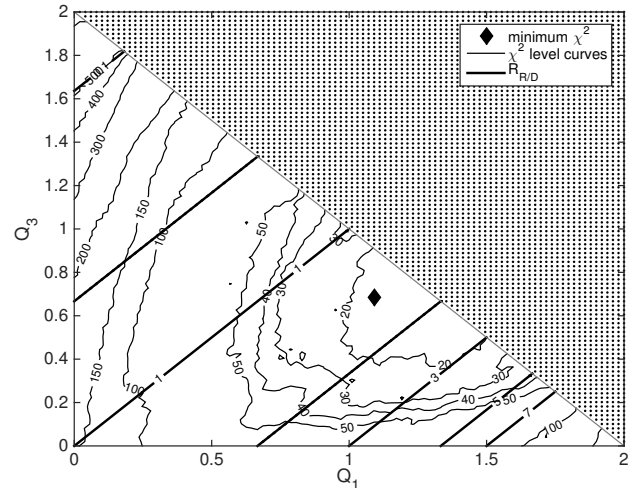

Fig. 10. Level curves of χ^2 and ratio for the PL distribution model with two parameters. Lines and markers are the same as in Fig. 9.

where n_p is the number of estimated parameters. To avoid small number statistics and after checking the stability of χ^2, we based our predicted distribution on 10^5 samples and the number of bins is $m = 11$.

7. Results

We first test the obliquity distribution parametric models with two independent parameters, that is, a three-bin distribution, a piecewise linear function with middle point in 0, and a quadratic function. To find the best fitting parameters, we scan a grid and compute χ^2 for each grid point. Figures 9–11 show the level curves of χ^2 as a function of the parameters.

Table 2 gives the best-fit χ^2, the p-value, that is, the probability of randomly obtaining a larger χ^2, and the corresponding ratio between retrograde and direct rotators. All the models provide statistically acceptable p-values, with a quadratic model giving the best fit with a χ^2 of 7.4.

All of the models give a retrograde to direct rotators ratio ($R_{R/D}$) that is statistically consistent with the $2^{+1}_{-0.7}$ ratio found

Table 2. Best-fit parameters, χ^2, p-value, and retrograde to direct rotators ratio ($R_{R/D}$) for the models with two independent parameters.

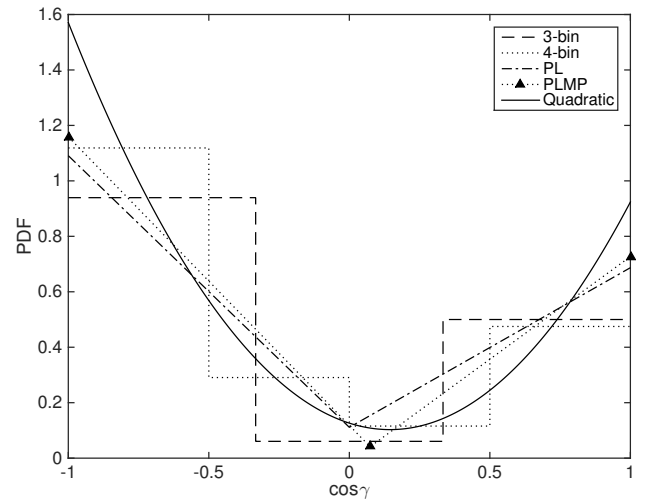|	Three-bin	Piecewise linear	Quadratic
Best-fit parameters	$p_1 = 0.63^{+0.09}_{-0.06}$	$Q_1 = 1.10^{+0.38}_{-0.02}$	$a = 1.12^{+0.21}_{-0.44}$
	$p_2 = 0.04^{+0.09}_{-0.04}$	$Q_2 = 0.11^{+0.08}_{-0.11}$	$b = -0.32^{+0.2}_{-0.14}$
	$p_3 = 0.33^{+0.03}_{-0.07}$	$Q_3 = 0.69^{+0.18}_{-0.24}$	$c = 0.13^{+0.15}_{-0.07}$
Minimum χ^2	13	10	7
p-value	9%	24%	49%
$R_{R/D}$	$1.8^{+0.8}_{-0.2}$	$1.5^{+1.4}_{-0.2}$	$2.0^{+0.8}_{-0.7}$

Notes. The error bars in the best-fit parameters and $R_{R/D}$ are at the 2σ level, that is, corresponding to the minimum and maximum values of the parameters for the grid points with a $\Delta\chi^2 \leq 4$ with respect to the best-fit solution.
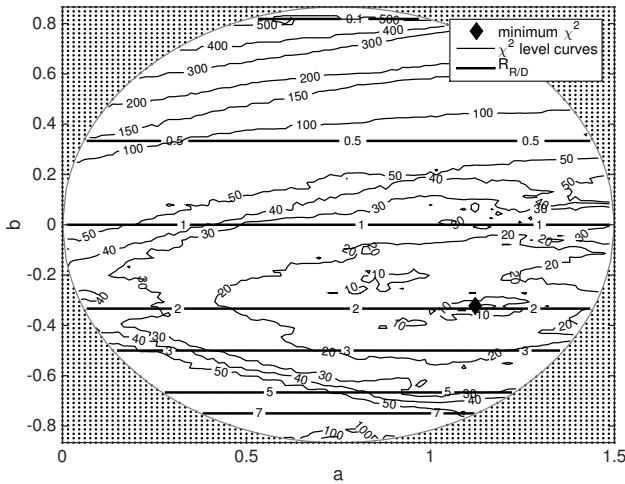
Fig. 11. Quadratic distribution: level curves of χ^2 and ratio in the 2D search space. Lines and markers are the same as in Fig. 9.

Fig. 12. Best-fit obliquity distributions for the three-bin, piecewise linear, quadratic, and four-bin models.

by La Spina et al. (2004) and also with the theoretical 2 ± 0.2 ratio derived from NEA population models (Bottke et al. 2002a), which suggests that NEAs generally maintain their rotation direction. However, if the timescales required to complete a YORP cycle (Rubincam 2000) are much shorter than the typical NEA dynamical lifetime, the YORP effect should have randomized the distribution of prograde versus retrograde rotators. YORP self-limitation (Cotto-Figueroa et al. 2015) may provide a means to reconcile the high present-day retrograde fraction, where the YORP-driven deformation of aggregate objects confines their rotation rates to far narrower ranges than would be expected in the classical YORP-cycle picture, therefore greatly prolonging the times over which objects can preserve their sense of rotation.

We now try to increase the number of independent parameters to three for the bin and piecewise linear models. Therefore, the expected χ^2 decreases to 7. To find an absolute minimum value of χ^2 on a three-dimensional (3D) space we use the IDEA global optimizer (Vasile et al. 2011). For a four-bin distribution we find a best fit solution $(p_1, p_2, p_3, p_4) = (0.56, 0.15, 0.06, 0.28)$ with minimum $\chi^2 = 9.55$ (p-value of 22%) and $R_{R/D} = 2.4$. An F-test shows that the $\Delta\chi^2 = 13.60 - 9.55$ improvement due to the addition of a third parameter is only significant at the 13% level. For the generalized piecewise linear function with variable mid-point abscissa the best fit solution is $(Q_1, Q_2, Q_3, x_2) = (1.16, 0.04, 0.73, 0.074)$ with minimum $\chi^2 = 8.14$ (p-value of 32%) and $R_{R/D} = 1.8$. Again, the statistical significance of $\Delta\chi^2 = 10.43 - 8.14$ as measured by an F-test is only 20%.

Therefore, the addition of a third parameter is only marginally significant and the quadratic model with two independent parameters provides the lowest χ^2. This suggests that our set of Yarkovsky estimates does not have enough signal to solve for more than two parameters.

Figure 12 shows the best-fit distribution obtained with the different models. Interestingly, all of the models favor extreme obliquities, which is consistent with the expected consequences of the YORP mechanism (Čapek & Vokrouhlický 2004). Figure 13 shows the corresponding distributions in normalized A_2 with that coming from the Yarkovsky estimates. All the models capture the bimodal behavior of the dataset of Yarkovsky estimates and find a larger fraction of negative A_2 values, which is consistent with the preliminary results from Cotto-Figueroa (2013). The distributions from our models overestimate the heights of the peaks of the A_2 distribution. Besides statistical noise due to Poisson statistics in the Yarkovsky sample, this effect could be caused by inaccurate assumptions in the distributions adopted in Sect. 4. For instance, the peaks drop by 10% when doubling the standard deviation of the density probability distributions in Table 1. However, the qualitative results on the obliquity distribution still stand; for example, the ratio between retrograde and direct rotators does not change.

Figure 14 compares the Farnocchia et al. (2013a) result with the distributions found in this paper. For this purpose we convert our best-fit distribution to a four-bin one by computing their integral over each of the four bins. Interestingly, Farnocchia et al. (2013a) found a ratio of 2.7 between retrograde and direct

Table 3. Comparison of the best-fit obliquity distributions with the known spin axes from the EARN and DAMIT databases.

	$\cos \gamma < -1/3$	$|\cos \gamma| \leq 1/3$	$\cos \gamma > 1/3$
EARN [Any H, 43 objects]	$(67 \pm 7)\%$	$(14 \pm 5)\%$	$(19 \pm 6)\%$
EARN [$H \leq 18$, 30 objects]	$(70 \pm 9)\%$	$(17 \pm 7)\%$	$(13 \pm 6)\%$
EARN [$H > 18$, 13 objects]	$(61 \pm 14)\%$	$(8 \pm 8)\%$	$(31 \pm 13)\%$
3-bin	$(63 \pm 1)\%$	$(4 \pm 2)\%$	$33^{+2}_{-1}\%$
4-bin	61%	13%	26%
PL	$51^{+6}_{-1}\%$	$16^{+1}_{-5}\%$	$33^{+1}_{-4}\%$
PLMP	54%	14%	32%
Quadratic	$59^{+2}_{-8}\%$	$11^{+6}_{-2}\%$	$(30 \pm 4)\%$

Notes. The error bars are 1σ. For the models with three independent parameters we do not have error bars as the best-fit solution was found with the IDEA global optimizer.
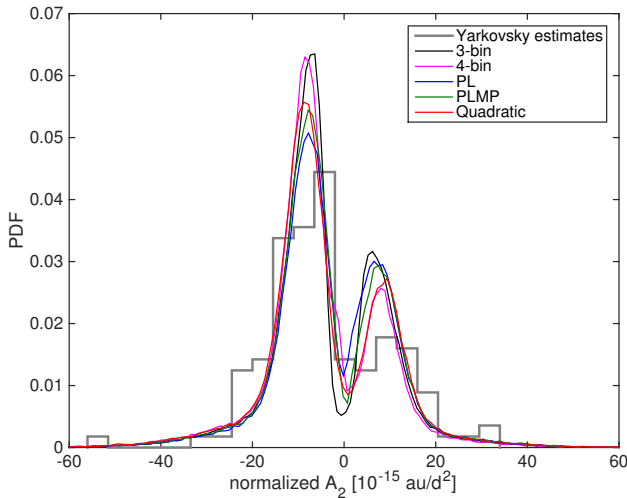
Fig. 13. Comparison between the probability distributions in normalized A_2 obtained from the Yarkovsky estimates and that from the different obliquity distribution models.

Fig. 14. Comparison between the obliquity distribution presented by Farnocchia et al. (2013a) and the four-bin split of our the best-fit obliquity distributions converted to four bins. In the legend we recall the ratio between retrograde and direct rotators $R_{\mathrm{R/D}}$.

Table 4. Best-fit χ^2 and p-values with enhancement factor $\alpha = 1$.

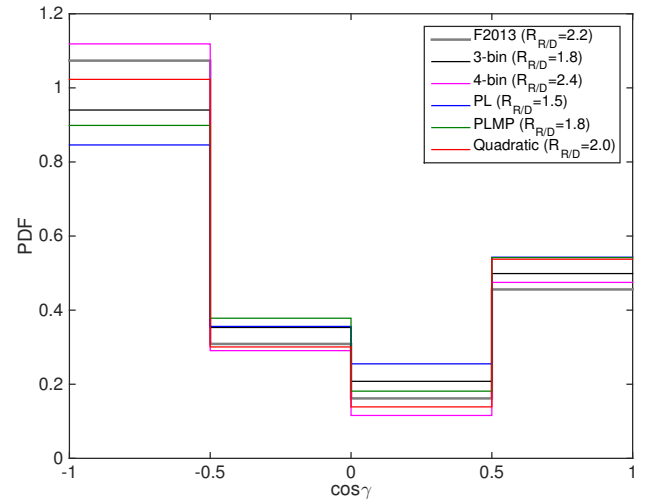| Distribution model	Minumum χ^2	p-value
3-bin	29.26	0.03%
4-bin	22.05	0.2%
PL	24.51	0.2%
PLMP	22.40	0.2%
Quadratic	19.23	1%

rotators, while our results are closer to the theoretical expectation, which further suggests that the technique used in this paper has higher fidelity.

To validate our results, we consider the known spin axes of 41 NEOs from the EARN database[4] and of 17 objects (15 already in the EARN database) from the DAMIT database[5]. Table 3 reports the fractions of obliquities with $\cos \gamma < -1/3$, $-1/3 < \cos \gamma < 1/3$, or $\cos \gamma > 1/3$. Since the objects in our dataset of Yarkovsky estimates had H in the range 14–29 with a peak around $H = 20$, Table 3 also shows the split for different H ranges. Larger objects ($H < 18$) have more mass in the middle bin than in that with $\cos \gamma > 1/3$. On the other hand, smaller objects have a smaller fraction of mid-range obliquities, which is again consistent with the YORP mechanism. It is interesting to point out that all of our best-fit solutions give a split that is well within 1σ of the observed obliquity distribution for objects with $H > 18$, which is also a condition that most objects of the Yarkovsky estimate dataset meet.

Finally, we check the significance of the Rozitis & Green (2012) enhancement factor α of the diurnal component of the Yarkovsky effect, discussed in Sect. 4. Table 4 gives the best-fit χ^2 and p-values for the different obliquity distributions obtained by setting $\alpha = 1$. For all of the models, the low p-values further

support the presence of a Yarkovsky enhancement factor as predicted by Rozitis & Green (2012).

8. Conclusions

We used the Chesley et al. (2016) list of Yarkovsky estimates to derive constraints on the obliquity distribution of near-Earth asteroids. We solved an inverse problem where we adopted probability distributions on the physical parameters other than obliquity (e.g., albedo, thermal inertia, bulk density) that determine the Yarkovsky effect. Then, we considered different parametric models for the probability density function of the cosine of the obliquity: piecewise constant (i.e., bins), piecewise linear, and quadratic functions. Finally, we performed χ^2 tests to quantify the goodness of the match to the distribution of the Yarkovsky estimates.

---

[4] http://earn.dlr.de/nea
[5] http://astro.troja.mff.cuni.cz/projects/asteroids3D/web.php

Using models with only two independent parameters seems to be the best compromise between model complexity and goodness of the fit. *F*-tests show that a third additional parameter is only marginally significant, thus suggesting that the dataset of Yarkovsky detections does not have enough resolution to constrain a third parameter. Among the analyzed obliquity distributions with two parameters, the one that produces the best-fit is obtained with a quadratic model: $f(\cos\gamma) = 1.12\cos^2\gamma - 0.32\cos\gamma + 0.13$. This solution favors extreme obliquities, which is consistent with the action of the YORP effect. Moreover, the corresponding ratio between retrograde and direct rotators, $2^{+0.4}_{-0.3}$, provides an excellent match to the La Spina et al. (2004) result, that is, $2^{+1}_{-0.7}$, and the Bottke et al. (2002a) theoretical expectation for feeding asteroids into the inner solar system, that is, 2 ± 0.2. Finally, this distribution is very much consistent with the set of known spin axis orientations.

It is possible that the results we obtained are affected by selection effects. In fact, the starting dataset of Yarkovsky detections is comprised of objects with a strong observational dataset, possibly including radar observations. Therefore, objects that have a more favorable observing geometry such as PHAs, dominate the dataset. In particular, all the objects had an aphelion larger than 1 au and so it is possible that Interior-Earth-Objects have a different obliquity distribution than what we derived. Future work will include assessing how this sort of orbital selection bias affects the extrapolation to the entire near-Earth asteroid population.

We also find that the current sweet spot for Yarkovsky detections is around $H = 20$, with most of the Yarkovsky estimates having an absolute magnitude between $H = 17$ and $H = 23$. Brighter objects are likely larger, making the Yarkovsky effect smaller and harder to detect. Fainter objects are less likely to be observed over a long time span, making them more difficult to discern.

The obliquity distribution outside of this magnitude range could be different. In particular, for near-Earth asteroids with known spin axes there is a larger fraction of mid-range obliquities for $H < 18$ than for $H > 18$. This difference could be caused by the $1/D^2$ dependence of the YORP effect (Vokrouhlický et al. 2015a), which makes it less effective at driving the spin to extreme obliquities on larger objects. On the other hand, the timescales of YORP cycles or stochastic YORP (Statler 2009) for objects smaller than the ones in our dataset can be shorter. Therefore, these objects would have a more frequent reconfiguration of the rotation state as the spin-up limit is reached.

Another limitation of our model is that we neglect non-principal-axis rotation. As discussed by Vokrouhlický et al. (2015b), for a tumbling asteroid, the Yarkovsky effect essentially depends on the rotational angular momentum rather than the spin axis. Therefore, if the fraction of non-principal-axis rotators were significant, our obliquity distribution would be more reflective of the orientation of the angular momentum vector than that of the spin axis.

The obliquity distributions presented here can be useful when an a priori distribution on the Yarkovsky perturbations is desired to model the trajectory of a target asteroid and no signal is yet visible from the orbital fit to the astrometry. This was the case for Apophis (Farnocchia et al. 2013b) and 2009 FD (Spoto et al. 2014) where the impact predictions are sensitive to the Yarkovsky effect though a direct estimate was not available.

References

Benner, L. A. M., Busch, M. W., Giorgini, J. D., Taylor, P. A., & Margot, J.-L. 2015, Radar Observations of Near-Earth and Main-Belt Asteroids, eds. P. Michel, F. E. DeMeo, & W. F. Bottke, 165

Bottke, W. F., Morbidelli, A., Jedicke, R., et al. 2002a, Icarus, 156, 399

Bottke, W. F., Vokrouhlický, D., Rubincam, D. P., & Broz, M. 2002b, Asteroids III (Tucson: University of Arizona Press), 395

Bottke, W. F., Vokrouhlický, D., Rubincam, D. P., & Nesvorný, D. 2006, Ann. Rev. Earth Planet. Sci., 34, 157

Bowell, E., Hapke, B., Domingue, D., et al. 1989, in Asteroids II, eds. R. P. Binzel, T. Gehrels, & M. S. Matthews, 524

Busch, M. W., Giorgini, J. D., Ostro, S. J., et al. 2007, Icarus, 190, 608

Čapek, D., & Vokrouhlický, D. 2004, Icarus, 172, 526

Carry, B. 2012, Planet. Space Sci., 73, 98

Chesley, S. R. 2006, in Asteroids, Comets, Meteors, eds. L. Daniela, M. Sylvio Ferraz, & F. J. Angel, IAU Symp., 229, 215

Chesley, S. R., Chodas, P. W., Milani, A., Valsecchi, G. B., & Yeomans, D. K. 2002, Icarus, 159, 423

Chesley, S. R., Ostro, S. J., Vokrouhlický, D., et al. 2003, Science, 302, 1739

Chesley, S. R., Farnocchia, D., Nolan, M. C., et al. 2014, Icarus, 235, 5

Chesley, S. R., Farnocchia, D., Pravec, P., & Vokrouhlický, D. 2016, in Asteroids: New Observations, New Models, eds. S. R. Chesley, A. Morbidelli, R. Jedicke, & D. Farnocchia, IAU Symp., 318, 250

Cotto-Figueroa, D. 2013, Ph.D. Thesis, Ohio University

Cotto-Figueroa, D., Statler, T. S., Richardson, D. C., & Tanga, P. 2015, ApJ, 803, 25

Delbò, M., Mueller, M., Emery, J. P., Rozitis, B., & Capria, M. T. 2015, Asteroid Thermophysical Modeling, eds. P. Michel, F. E. DeMeo, & W. F. Bottke, 107

Ďurech, J., Kaasalainen, M., Warner, B. D., et al. 2009, A&A, 493, 291

Ďurech, J., Kaasalainen, M., Herald, D., et al. 2011, Icarus, 214, 652

Farinella, P., Vokrouhlický, D., & Hartmann, W. K. 1998, Icarus, 132, 378

Farnocchia, D., & Chesley, S. 2014, Icarus, 229, 321

Farnocchia, D., Chesley, S., Vokrouhlický, D., et al. 2013a, Icarus, 224, 1

Farnocchia, D., Chesley, S. R., Chodas, P. W., et al. 2013b, Icarus, 224, 192

Farnocchia, D., Chesley, S. R., Tholen, D. J., & Micheli, M. 2014, Celes. Mech. Dyn. Astron., 119, 301

Farnocchia, D., Chesley, S. R., Milani, A., Gronchi, G. F., & Chodas, P. W. 2015, Orbits, Long-Term Predictions, Impact Monitoring, eds. P. Michel, F. E. DeMeo, & W. F. Bottke, 815

Giorgini, J., Ostro, S., Benner, L., et al. 2002, Science, 296, 132

Giorgini, J. D., Benner, L. A., Ostro, S. J., Nolan, M. C., & Busch, M. W. 2008, Icarus, 193, 1

La Spina, A., Paolicchi, P., Kryszczyńska, A., & Pravec, P. 2004, Nature, 428, 400

Mommert, M., Farnocchia, D., Hora, J. L., et al. 2014a, ApJ, 789, L22

Mommert, M., Hora, J. L., Farnocchia, D., et al. 2014b, ApJ, 786, 148

Morbidelli, A., & Vokrouhlický, D. 2003, Icarus, 163, 120

Nugent, C. R., Margot, J. L., Chesley, S. R., & Vokrouhlický, D. 2012, AJ, 144, 60

Pravec, P., & Harris, A. W. 2007, Icarus, 190, 250

Rozitis, B., & Green, S. F. 2012, MNRAS, 423, 367

Rubincam, D. P. 2000, Icarus, 148, 2

Spoto, F., Milani, A., Farnocchia, D., et al. 2014, A&A, 572, A100

Statler, T. S. 2009, Icarus, 202, 502

Thomas, C. A., Trilling, D. E., Emery, J. P., et al. 2011, AJ, 142, 85

Vasile, M., Minisci, E., & Locatelli, M. 2011, IEEE Trans. Evolutionary Computation, 15, 267

Vokrouhlický, D., Chesley, S. R., & Matson, R. D. 2008, AJ, 135, 2336

Vokrouhlický, D., Bottke, W. F., Chesley, S. R., Scheeres, D. J., & Statler, T. S. 2015a, The Yarkovsky and YORP Effects, eds. P. Michel, F. E. DeMeo, & W. F. Bottke, 509

Vokrouhlický, D., Farnocchia, D., Čapek, D., et al. 2015b, Icarus, 252, 277

Warner, B. D., Harris, A. W., & Pravec, P. 2009, Icarus, 202, 134

Appendix A: Additional table

Table A.1. List of Yarkovsky estimates as of September 2016.

Object		H	A_2 (10^{-15} au/d^2)	Object		H	A_2 (10^{-15} au/d^2)
101955	Bennu	20.6	-45.50 ± 0.24	401885	2001 RV17	20.3	-38.46 ± 17.44
2340	Hathor	20.2	-30.17 ± 1.21	306383	1993 VD	21.6	-22.18 ± 10.43
152563	1992 BF	19.7	-24.57 ± 1.17		2009 WB105	23.6	93.78 ± 44.49
	2009 BD	28.2	-1143.29 ± 79.02	6037	1988 EG	18.7	-19.06 ± 9.06
	2005 ES70	23.7	-128.48 ± 8.94		1991 GO	19.9	-39.34 ± 18.89
437844	1999 MN	21.4	40.84 ± 4.33	164202	2004 EW	20.7	60.90 ± 29.29
468468	2004 KH17	21.9	-66.02 ± 8.16	297418	2000 SP43	18.5	-27.30 ± 13.14
85990	1999 JV6	20.1	-30.30 ± 3.85	385186	1994 AW1	17.5	14.08 ± 6.87
2062	Aten	17.1	-12.54 ± 1.62	162361	2000 AF6	20.0	32.91 ± 16.26
6489	Golevka	19.1	-10.82 ± 1.43	154590	2003 MA3	21.7	-79.82 ± 39.78
162004	1991 VE	18.2	24.63 ± 3.74		2005 GR33	22.2	-110.65 ± 55.92
1862	Apollo	16.1	-3.02 ± 0.47	416151	2002 RQ25	20.5	49.60 ± 25.15
	2006 CT	22.3	-110.55 ± 17.81	164207	2004 GU9	21.1	-71.23 ± 37.73
	2003 YL118	21.6	-177.54 ± 29.19	467336	2002 LT38	20.5	22.83 ± 12.17
	1999 UQ	21.5	-111.92 ± 18.50	330659	2008 GG2	22.8	56.80 ± 30.53
33342	1998 WT24	17.9	-26.75 ± 4.46	250680	2005 QC5	19.7	24.02 ± 13.10
326290	Akhenaten	21.7	-66.68 ± 11.20	6239	Minos	18.4	13.50 ± 7.46
	2000 PN8	22.1	123.81 ± 21.89	152664	1998 FW4	19.7	18.91 ± 10.76
455176	1999 VF22	20.6	-84.51 ± 15.20		2004 BG41	24.4	-120.76 ± 70.12
	2001 BB16	23.1	400.40 ± 74.11	443837	2000 TJ1	19.3	-29.62 ± 17.42
216523	2001 HY7	20.4	59.36 ± 11.21	152756	1999 JV3	18.9	17.82 ± 10.70
10302	1989 ML	19.4	75.36 ± 14.48	369986	1998 SO	20.6	21.13 ± 12.88
3908	Nyx	17.3	23.79 ± 4.63	163348	2002 NN4	20.0	29.50 ± 18.28
85953	1999 FK21	18.0	-10.60 ± 2.15	137924	2000 BD19	17.2	-9.73 ± 6.36
	1995 CR	21.7	-172.49 ± 36.23	5381	Sekhmet	16.4	7.09 ± 4.74
1685	Toro	14.3	-2.95 ± 0.62	136770	1996 PC1	20.4	-18.94 ± 12.92
29075	1950 DA	17.1	-6.12 ± 1.31	364136	2006 CJ	20.2	-20.24 ± 14.55
2100	Ra-Shalom	16.2	-9.12 ± 1.98	422686	2000 AC6	21.3	38.57 ± 27.92
399308	1993 GD	20.7	101.19 ± 22.41	337248	2000 RH60	20.0	-20.60 ± 15.34
363505	2003 UC20	18.3	-7.60 ± 1.73	4660	Nereus	18.1	12.91 ± 9.66
4034	Vishnu	18.3	-74.44 ± 17.21	469445	2002 LT24	21.9	-38.75 ± 29.50
363599	2004 FG11	21.0	-53.46 ± 12.68	2063	Bacchus	17.2	-7.18 ± 5.64
377097	2002 WQ4	19.5	-23.60 ± 5.92	172034	2001 WR1	17.7	-10.25 ± 8.21
425755	2011 CP4	21.1	65.67 ± 16.66	138258	2000 GD2	19.1	-28.53 ± 22.98
	1994 XL1	20.8	-53.55 ± 13.74	11054	1991 FA	16.8	-4.19 ± 3.38
3361	Orpheus	19.0	14.80 ± 3.81	141531	2002 GB	19.0	27.56 ± 23.44
397326	2006 TC1	19.0	34.75 ± 9.14	1620	Geographos	15.2	-1.95 ± 1.70
138852	2000 WN10	20.1	37.32 ± 9.86		2005 QQ87	22.6	67.80 ± 59.12
	2008 CE119	25.6	-143.48 ± 38.08		2000 YA	23.8	-110.26 ± 100.50
85774	1998 UT18	19.1	-6.15 ± 1.64	373393	1972 RB	19.2	13.13 ± 14.51
99907	1989 VA	17.8	17.61 ± 4.70	87309	2000 QP	17.5	-10.13 ± 11.59
1566	Icarus	16.3	-2.82 ± 0.75	277810	2006 FV35	21.7	21.37 ± 25.70
138175	2000 EE104	20.2	-67.27 ± 18.47	339714	2005 ST1	20.3	-14.22 ± 17.75
	2008 BX2	23.7	-222.01 ± 61.18	1221	Amor	17.5	-2.06 ± 2.79
66400	1999 LT7	19.4	-49.23 ± 14.22		2014 UR	26.1	-119.63 ± 162.79
4581	Asclepius	20.7	-40.51 ± 11.73		2003 XV	26.6	-222.75 ± 340.76
	2007 TF68	22.7	-156.33 ± 45.74	376879	2001 WW1	21.9	-24.66 ± 39.38
136818	Selqet	19.1	22.09 ± 6.61	25143	Itokawa	18.9	-11.94 ± 19.40
4179	Toutatis	15.1	-4.45 ± 1.34	86667	2000 FO10	17.6	-5.83 ± 10.17
256004	2006 UP	23.0	-190.85 ± 58.18	225312	1996 XB27	21.7	-13.54 ± 25.77
350462	1998 KG3	22.2	-63.41 ± 19.61		2009 TK	22.3	-22.81 ± 44.76
441987	2010 NY65	21.5	-36.90 ± 11.50	422638	1994 CB	21.1	-10.73 ± 23.34
	1999 SK10	19.6	-54.80 ± 17.40	5797	Bivoj	18.8	-3.79 ± 9.36
54509	YORP	22.6	-90.22 ± 30.08	52381	1993 HA	20.1	6.05 ± 16.03
85770	1998 UP1	20.4	-36.47 ± 12.26	345705	2006 VB14	18.6	-7.19 ± 19.47
152671	1998 HL3	20.0	-64.51 ± 21.74	276033	2002 AJ129	18.5	3.03 ± 8.23
37655	Illapa	17.8	-12.37 ± 4.28		2000 TH1	22.5	-12.89 ± 41.72
310442	2000 CH59	19.7	38.50 ± 13.60	152742	1998 XE12	19.0	4.41 ± 14.46
162181	1999 LF6	18.2	-21.86 ± 7.98	247517	2002 QY6	19.6	4.76 ± 15.81
267759	2003 MC7	18.7	-28.81 ± 10.62		2008 HU4	28.3	-45.26 ± 171.36
	2005 EY169	22.1	-123.37 ± 49.48	3757	Anagolay	19.1	-0.19 ± 12.42
230111	2001 BE10	19.0	-26.13 ± 10.83	161989	Cacus	17.2	0.06 ± 4.97
41429	2000 GE2	20.4	-81.54 ± 34.31				